Research Article Vol. 36, No. 2 / February 2019 / Journal of the Optical Society of America A 253

Journal of the Optical Society of America A

OPTICS, IMAGE SCIENCE, AND VISION

Diffraction from two-dimensional orthogonal nonseparable periodic structures: Talbot distance dependence on the number theoretic properties of the structures

Davud Hebri[1] and Saifollah Rasouli[1,2,*]

[1]Department of Physics, Institute for Advanced Studies in Basic Sciences (IASBS), Zanjan 45137-66731, Iran
[2]Optics Research Center, Institute for Advanced Studies in Basic Sciences (IASBS), Zanjan 45137-66731, Iran
*Corresponding author: rasouli@iasbs.ac.ir

Received 19 November 2018; revised 1 January 2019; accepted 2 January 2019; posted 3 January 2019 (Doc. ID 352341); published 25 January 2019

In this work, the diffraction-based discrimination of two-dimensional (2D) orthogonal separable and nonseparable periodic structures and prediction of the reduced Talbot distances for 2D orthogonal nonseparable periodic structures are presented. 2D orthogonal periodic structures are defined and classified into separable (multiplicative or additive) and nonseparable categories with the aid of a spatial spectrum lattice. For both the separable and nonseparable cases, the spatial spectra or far-field impulses are 2D orthogonal lattices. We prove that for a 2D orthogonal separable structure, in addition to the DC impulse, there are other impulses on the coordinate axes. As a result, if all the spectrum impulses of a structure on the coordinate axes, except for the DC impulse, vanish, we conclude that the structure is nonseparable. In the second part of this work, using a unified formulation, the near-field diffraction of the 2D orthogonal separable and nonseparable periodic structures is investigated. In general, the Talbot distance equals the least common multiple of the individual Talbot distances in the orthogonal directions, say, $z_t = z_{\mathrm{lcm}}$. For the 2D orthogonal nonseparable periodic structures having Fourier coefficients only with odd indices, we have found surprising results. It is shown that for this kind of structure, the Talbot distance strongly depends on the number theoretic properties of the structure. Depending on the ratio of the structure's periods in the orthogonal directions, $\frac{p_x}{p_y}$, the Talbot distance reduces to $\frac{z_{\mathrm{lcm}}}{2}$, $\frac{z_{\mathrm{lcm}}}{4}$, or $\frac{z_{\mathrm{lcm}}}{8}$. In addition, for the 2D orthogonal nonseparable sinusoidal grating, we show that, regardless of the value of $\frac{p_x}{p_y}$, self-images are formed at distances smaller than the conventional Talbot distances attributed to p_x and p_y that we name the reduced Talbot (RT) distances. Halfway between two adjacent RT distances, the formation of negative self-images with a complementary amplitude of the self-images is predicted. Halfway between two adjacent self-image and negative-elf-image, subimages are formed. As another interesting result, we show that the intensity patterns of the subimages are 2D multiplicatively separable with halved periods in both directions. Finally, we show that 2D almost periodic structures with impulses on zone-plate-like concentric circles have self-images under plane wave illumination.

https://doi.org/10.1364/JOSAA.36.000253

1. INTRODUCTION

Periodic structures, including one-dimensional (1D) and two-dimensional (2D) gratings, have numerous applications in optics and metrology, such as in spectrometry, shearing interferometry [1–3], the optical alignment technique, and lithography [4–6]. Another important measurement technique that serves a pair of gratings or more is the moiré technique [7–10]. This technique is used in a variety of ways and for various applications such as moiré deflectometry, moiré topography, displacement and vibration measurements [11], strain and stress analysis, wavefront sensing, and 3D displays [12,13]. On the other hand, diffraction from periodic structures is an interesting topic and is now widely used in optics. For more than half a century, the physics of diffraction from 1D periodic structures has attracted much attention and has had many studies allocated to it [14–31]. But compared with the 1D case, few studies have been devoted to diffraction from 2D periodic structures [32–36].

2D orthogonal periodic structures can be classified into separable (including multiplicative and additive) and nonseparable

cases. For both separable and nonseparable cases, the spatial spectra of the structures are 2D orthogonal lattices. In this work, we show that the separability of the structure into two distinct 1D structures can be recognized from the far-field diffraction pattern of a given periodic structure that shows the spatial spectrum. It is shown that, for a 2D orthogonal separable structure, if the DC impulse exists, then there are other impulses on the coordinate axes. Accordingly, we deduce that if all the far-field impulses on the coordinate axes, excluding the DC one, vanish, then the structure is nonseparable. But the converse of the above statements is not necessarily true, meaning that when in addition to the DC impulse there are other impulses on the coordinate axes, then both separable and nonseparable cases are possible. In such a situation, again the separability of the structure can be determined from the investigation of the resulting spatial spectrum. We have recently proved that for a multiplicatively separable (MS) structure, its far-field diffraction pattern remains separable too [35]. Similarly, for an additively separable (AS) structure, its far-field diffraction pattern is also AS into two 1D spectra. Thus for the mentioned situation, the separability of the spatial spectrum pattern into two 1D structures determines the separability of the structure. Investigation of various behaviors of the near-field diffractions from separable and nonseparable structures also has some significant value in the field. In the second part of this work, we briefly present a unified formulation for the Talbot effect of 2D orthogonal separable and nonseparable periodic structures. As an example, near-field diffraction from a 2D orthogonal nonseparable sinusoidal grating is formulated, and more details are presented. It is worth mentioning that the case of MS periodic structures was already investigated with the aid of the contrast variation method in [35]. In that work, for a 2D MS sinusoidal structure, it was predicted that there would be additional self-images in addition to the Talbot images located at the least common multiple (LCM) of each of the individual 1D Talbot distances. Also, a study on Talbot images and the Talbot spectra of a 2D orthogonal periodic structure was presented in [34]. Here we show that for a 2D orthogonal nonseparable sinusoidal grating, its self-images are formed at the RT distances, which are smaller than the conventional Talbot distances corresponding to the periods in the x and y directions. As well as the halfway distance between two adjacent RTs, negative self-image formation with the complementary amplitude of the self-images is predicted. Most importantly, half-period 2D MS subimages are formed halfway between an adjacent self-image and a negative self-image.

In addition, for a 2D orthogonal nonseparable periodic structure having Fourier coefficients with only odd indices, we show that the Talbot distance depends strongly on the number theoretic properties of the structure. We show both theoretically and through computational simulations that, depending on the ratio of the structure's periods in the orthogonal directions, $\frac{p_x}{p_y}$, the Talbot distance reduces to $\frac{z_{\mathrm{lcm}}}{2}$, $\frac{z_{\mathrm{lcm}}}{4}$, or $\frac{z_{\mathrm{lcm}}}{8}$.

Finally, in Appendix A, it is shown that 2D almost periodic structures having impulses on zone-plate-like concentric circles form Talbot images, and as a typical example, we investigate the near-field diffraction from an octagonal almost periodic pure amplitude sinusoidal structure.

2. 2D ORTHOGONAL SEPARABLE AND NONSEPARABLE PERIODIC STRUCTURES

Now let us define 2D orthogonal separable and nonseparable periodic structures by the spatial spectrum concept. We define a 2D orthogonal periodic structure by a transmission function $t(x,y)$ that is a twofold periodic function in $\mathbb{R}^2$. It means that $t(x,y)$ is periodic in both the x and y directions with periods p_x and p_y, respectively [9]:

$$t(x+p_x,y)=t(x,y) \quad \text{and} \quad t(x,y+p_y)=t(x,y), \quad \text{for all } (x,y)\in\mathbb{R}^2.$$

Then $t(x,y)$ can be expanded into a 2D Fourier series [9]:

$$t(x,y)=\sum_{m,n=-\infty}^{+\infty} t_{m,n}\exp\left[2\pi i\left(\frac{m}{p_x}x+\frac{n}{p_y}y\right)\right], \tag{1}$$

where $t_{m,n}$ indicate Fourier coefficients. The spatial spectrum of the structure can be obtained by taking a 2D Fourier transform. Using 2D impulse symbol $\delta(\xi,\eta)$ one can write the spatial spectrum of the structure as

$$T(\xi,\eta)=\sum_{m,n=-\infty}^{+\infty} t_{m,n}\delta(\xi-mf_x,\eta-nf_y), \tag{2}$$

where $f_x=\frac{1}{p_x}$ and $f_y=\frac{1}{p_y}$ are the fundamental frequencies of the structure in the x and y directions, respectively. It indicates a 2D amplitude-modulated impulse comb in the spectral domain. The resulting impulse comb, or, equally, the spectrum pattern, is a 2D orthogonal lattice, where (m,n)th impulse is located at (mf_x,nf_y) with amplitude $t_{m,n}$. Consider two linearly independent vectors $\mathbf{V_1}$ and $\mathbf{V_2}$ in $\mathbb{R}^2$. The set of all points indicated by the end of vectors $\mathbf{V_{mn}}=m\mathbf{V_1}+n\mathbf{V_2}, m,n\in\mathbb{Z}$, is called a 2D lattice that we show by L. For the case $\mathbf{V_1}$ and $\mathbf{V_2}$ to be orthogonal, L is a 2D orthogonal lattice. A structure is 2D orthogonal periodic when its spatial spectrum is a 2D orthogonal lattice. As the far-field diffraction of a given structure is equal to its spatial spectrum, each 2D orthogonal lattice at far field corresponds to a 2D orthogonal periodic structure. 2D orthogonal periodic structures can be divided in two categories of separable and nonseparable. In this regard, the direction of coordinate system xa€ y is most important and is uniquely chosen so that in the spectral domain corresponding coordinate system $\xi-\eta$ to be parallel to the sides of the impulse lattice (see Fig. 1).

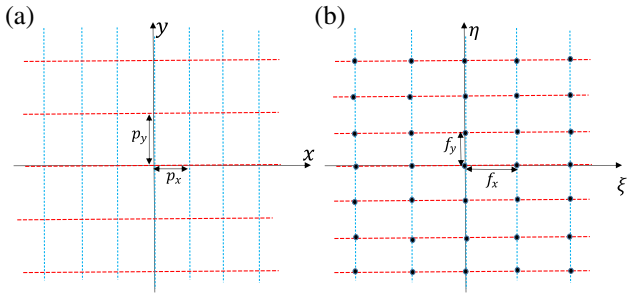

Fig. 1. (a) Schematic plot of a typical 2D orthogonal periodic structure in the spatial domain, and (b) its impulse lattice in the spectral domain.

Now we determine separability or nonseparability of a given structure into two distinct 1D structures from its spectrum. A structure is called 2D orthogonal MS or AS periodic structure when its transmission function, $t(x,y)$, can be written as the product or addition of two 1D periodic functions, $t_x(x)$ and $t_y(y)$, respectively:

$$t_{\mathrm{MS}}(x,y) = t_x(x)t_y(y), \qquad t_{\mathrm{AS}}(x,y) = t_x(x) + t_y(y). \tag{3}$$

In the other situations, the structure will be nonseparable. As $t_x(x)$ and $t_y(y)$ are periodic functions, their 1D Fourier transforms can be written, respectively, by

$$T_x(\xi) = \sum_{m=-\infty}^{+\infty} t_{xm}\delta(\xi - mf_x),$$
$$T_y(\eta) = \sum_{n=-\infty}^{+\infty} t_{yn}\delta(\eta - nf_y), \tag{4}$$

where t_{xm} and t_{yn} are Fourier coefficients. Now, using separable product theorem [9,35], the spectra of t_{MS} and t_{AS} are obtained as

$$\begin{aligned} T_{\mathrm{MS}}(\xi,\eta) = {} & t_{x0}t_{y0}\delta(\xi)\delta(\eta) + t_{y0}\delta(\eta)\sum_{m\neq 0} t_{xm}\delta(\xi - mf_x) \\ & + t_{x0}\delta(\xi)\sum_{n\neq 0} t_{yn}\delta(\eta - nf_y) \\ & + \sum_{m,\,n\neq 0} t_{xm}t_{yn}\delta(\xi - mf_x)\delta(\eta - nf_y), \end{aligned} \tag{5}$$

$$\begin{aligned} T_{\mathrm{AS}}(\xi,\eta) = {} & (t_{x0} + t_{y0})\delta(\xi)\delta(\eta) \\ & + \delta(\eta)\sum_{m\neq 0} t_{xm}\delta(\xi - mf_x) + \delta(\xi)\sum_{n\neq 0} t_{yn}\delta(\eta - nf_y). \end{aligned} \tag{6}$$

Obviously, for both MS and AS structures, if there exists a DC term, say, $t_{x0} \neq 0$ and $t_{y0} \neq 0$, in addition to the DC impulse (first term) there are other impulses on the coordinate axes (second and third terms). The contrapositive of this statement is "if all of the far-field impulses on the coordinate axes excluding the DC one vanish, then the structure is nonseparable." Here, to clarify the subject, we examine three 2D orthogonal MS, AS, and (multiplicatively and additively) nonseparable sinusoidal amplitude gratings in the x and y directions, respectively:

$$t_{\mathrm{MS}}(x,y) = \frac{1}{2}\left[1 + \alpha_x \cos\left(\frac{2\pi x}{p_x}\right)\right] \times \frac{1}{2}\left[1 + \alpha_y \cos\left(\frac{2\pi x}{p_y}\right)\right], \tag{7}$$

$$t_{\mathrm{AS}}(x,y) = \frac{1}{4}\left[1 + \alpha_x \cos\left(\frac{2\pi x}{p_x}\right)\right] + \frac{1}{4}\left[1 + \alpha_y \cos\left(\frac{2\pi y}{p_y}\right)\right], \tag{8}$$

$$t_{\mathrm{NS}}(x,y) = \frac{1}{2}\left[1 + \alpha \cos\left(\frac{2\pi x}{p_x}\right)\cos\left(\frac{2\pi y}{p_y}\right)\right], \tag{9}$$

where α is a real parameter, and NS stands for the nonseparable structure. Figure 2 shows these structures and their corresponding spectra in the frequency domain.

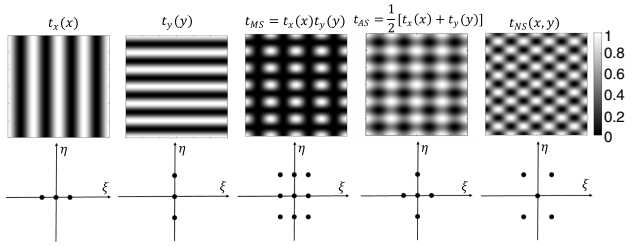

Fig. 2. Two typical 1D sinusoidal structures (having DC term) in the x and y directions with different periods, their product, their summation, and a typical 2D orthogonal (multiplicatively and additively) nonseparable sinusoidal structure (first row, left to right); their corresponding spectra in the frequency domain (second row). The gray scale is for all of images.

3. TALBOT EFFECT OF 2D ORTHOGONAL PERIODIC STRUCTURES

Here we consider the near-field diffraction from a 2D orthogonal periodic structure defined previously. By illuminating the structure with a coherent uniform light beam, according to Eq. (1), the field distribution immediately after the structure can be written by

$$u_0(x,y) = \sum_{m,\,n=-\infty}^{+\infty} t_{m,n} \exp[2\pi i(mf_x x + nf_y y)]. \tag{10}$$

The corresponding spatial spectrum is

$$U_0(\xi,\eta) = \sum_{m,\,n=-\infty}^{+\infty} t_{m,n}\delta(\xi - mf_x, \eta - nf_y). \tag{11}$$

By multiplying this expression to the free space transfer function in Fresnel approximation [37],

$$H(\xi,\eta) = H_0 \exp[-i\pi\lambda z(\xi^2 + \eta^2)], \tag{12}$$

we can get the spatial spectrum at the output plane at distance z from the structure:

$$\begin{aligned} U_z(\xi,\eta) = {} & \sum_{m,\,n=-\infty}^{+\infty} t_{m,n} \exp[-i\pi\lambda z(\xi^2 + \eta^2)] \\ & \times \delta(\xi - mf_x, \eta - nf_y), \end{aligned} \tag{13}$$

where, for convenience, we ignored $H_0 = e^{ikz}$. By taking 2D inverse Fourier transform from Eq. (13), one can obtain amplitude field distribution at distance z from the structure

$$\begin{aligned} u_z(x,y) = {} & \sum_{m,\,n=-\infty}^{+\infty} t_{m,n} \exp[2\pi i(mf_x x + nf_y y)] \\ & \times \exp[-i\pi\lambda z(m^2 f_x^2 + n^2 f_y^2)]. \end{aligned} \tag{14}$$

By defining $z_{tx} = \frac{2}{\lambda f_x^2}$ and $z_{ty} = \frac{2}{\lambda f_y^2}$ as the Talbot distances attributed to the structure periods in the x and y directions, Eq. (14) can be written as

$$\begin{aligned} u_z(x,y) = {} & \sum_{m,\,n=-\infty}^{+\infty} t_{m,n} \exp[2\pi i(mf_x x + nf_y y)] \\ & \times \exp\left[-i2\pi z\left(\frac{m^2}{z_{tx}} + \frac{n^2}{z_{ty}}\right)\right]. \end{aligned} \tag{15}$$

Assuming $\frac{z_{tx}}{z_{ty}} = (\frac{p_x}{p_y})^2$ to be a rational number, then we can write

$$\frac{z_{tx}}{z_{ty}} = \left(\frac{p_x}{p_y}\right)^2 = \frac{k}{l}, \tag{16}$$

where l and k are relatively prime positive integer numbers. Let us now define $z_{\mathrm{lcm}} = lz_{tx} = kz_{ty}$ as the 2D structure Talbot distance that is the LCM of z_{tx} and z_{ty}. Accordingly, we can rewrite Eq. (15) as

$$u_z(x,y) = \sum_{m,n=-\infty}^{+\infty} t_{m,n} \exp[2\pi i(mf_x x + nf_y y)] \times \exp\left[-2\pi i\left(\frac{z}{z_{\mathrm{lcm}}}\right)(lm^2 + kn^2)\right]. \tag{17}$$

As $(lm^2 + kn^2)$ is always an integer number, at distances equal to integer multiples of z_{lcm}, namely, $z_q = qz_{\mathrm{lcm}}$, $q = 1, 2, 3, \ldots$, the light beam amplitude exactly recovers its initial shape:

$$u_{z=z_q}(x,y) = u_0(x,y). \tag{18}$$

Then, for any 2D orthogonal periodic structure, consisting of both separable and nonseparable cases, at these distances self-images are formed.

Let us now consider a special case in which $p_x = \sqrt{q}p_y$, where $q = 1, 2, 3, \ldots$. Using Eq. (16), we get $\frac{z_{tx}}{z_{ty}} = q$. For such a structure, $z_{\mathrm{lcm}} = z_{tx} = \frac{2p_x^2}{\lambda}$, and therefore the Talbot distance does not depend on p_y. A comprehensive interpretation in the spectral domain for this effect is presented in Section C of Appendix A.

In the rest of the paper, for simplicity we consider a sinusoidal amplitude 2D orthogonal NS structure defined by Eq. (9). It worth mentioning that the case of MS periodic structures was already investigated by the aid of contrast variation method in [35]. In that work, for a 2D MS sinusoidal structure defined in Eq. (7) (see Fig. 2, first row, third column), it has been predicted that there are additional self-images, in addition to the Talbot images located at the LCM of each of the individual 1D Talbot distances, z_{lcm}. Also, it was shown that the diffraction pattern of a 2D MS sinusoidal structure depends strongly on the ratio square of 1D structures' periods in the x and y directions.

4. RT DISTANCES FOR 2D ORTHOGONAL NONSEPARABLE STRUCTURES

A. Nonseparable Sinusoidal Gratings

Now let us come back to Eq. (9); by illuminating such a 2D nonseparable sinusoidal grating by a coherent uniform light beam, the transmitted amplitude is

$$u_0(x,y) = \frac{1}{2}[1 + \alpha \cos(2\pi f_x x)\cos(2\pi f_y x)]. \tag{19}$$

It can be rewritten in an exponential form as

$$u_0(x,y) = t_{0,0} + \sum_{m,n=\pm 1} t_{m,n} \exp[2\pi i(mf_x x + nf_y y)], \tag{20}$$

where $t_{0,0} = \frac{1}{2}$ and for the other four terms, $t_{m,n} = \frac{\alpha}{8}$. By comparison with Eq. (10) and using Eq. (17), the complex amplitude of the light beam after propagation can be obtained as

$$u_z(x,y) = t_{0,0} + \exp\left[-i2\pi\left(\frac{z}{z_{\mathrm{lcm}}}\right)(l+k)\right] \times \sum_{m,n=\pm 1} t_{m,n} \exp[2\pi i(mf_x x + nf_y y)]. \tag{21}$$

Let us define a new distance parameter z_{RT} by

$$z_{\mathrm{RT}} = \frac{z_{\mathrm{lcm}}}{l+k} = \frac{z_{tx}z_{ty}}{z_{tx} + z_{ty}}. \tag{22}$$

As z_{RT} is smaller than both z_{tx} and z_{ty}, we call it the RT distance. By replacing z_{RT} in Eq. (21) and rewriting it in cosine form we have

$$u_z(x,y) = \frac{1}{2}\left[1 + \alpha e^{-i2\pi(\frac{z}{z_{\mathrm{RT}}})} \cos\left(\frac{2\pi x}{p_x}\right)\cos\left(\frac{2\pi y}{p_y}\right)\right]. \tag{23}$$

By comparing the amplitude immediately after the grating, Eq. (19), and the diffracted one, Eq. (23), it is evident that at the distances equal to integer multiples of z_{RT}, namely, at $z_q = qz_{\mathrm{RT}}, q = 1, 2, 3, \ldots$, the light beam amplitude fully recovers its initial shape, $u_{z=z_q}(x,y) = u_0(x,y)$. Halfway between two successive RT distances, $z_{H,q} = (q - \frac{1}{2})z_{\mathrm{RT}}$, which we name reduced half-Talbot (RHT) distances, we have

$$u_{z=z_{H,q}}(x,y) = \frac{1}{2}\left[1 - \alpha \cos\left(\frac{2\pi x}{p_x}\right)\cos\left(\frac{2\pi y}{p_y}\right)\right]. \tag{24}$$

Here again, by comparing equations Eqs. (19) and (24), it can be concluded that

$$u_{z=z_{H,q}}(x,y) = u_0\left(x - \frac{p_x}{2}, y\right) = u_0\left(x, y - \frac{p_y}{2}\right). \tag{25}$$

It means that the resulting diffracted amplitude pattern can be considered the same as the transmitted amplitude for the grating with a half-period shift in the x or y direction (see Fig. 3). Moreover, halfway between two successive RHT distances, we call it reduced quarter-Talbot (RQT) distances, $z_{Q,n} = (n - \frac{1}{2})\frac{z_{\mathrm{RT}}}{2}, n = 1, 2, 3, \ldots$, and we have

$$u_{z=z_{Q,n}}(x,y) = \frac{1}{2}\left[1 + i(-1)^n \alpha \cos\left(\frac{2\pi x}{p_x}\right)\cos\left(\frac{2\pi y}{p_y}\right)\right]. \tag{26}$$

Now, the resulting intensity pattern is given by

$$I_{z=z_{Q,n}}(x,y) = \frac{1}{4} + \left[1 + \cos\left(\frac{2\pi x}{p_x/2}\right)\right] \times \left[1 + \cos\left(\frac{2\pi y}{p_y/2}\right)\right]. \tag{27}$$

Focusing on this equation, we see that at the RQT distances, the resulting intensity pattern can be considered as a 2D MS pattern after subtracting the background term (see Fig. 3). Second, despite the fact that the resulting intensity pattern periods in both the x and y directions are halved, still the phase map periods remain unchanged. By defining $g(x,y) = \alpha \cos(\frac{2\pi x}{p_x})\cos(\frac{2\pi y}{p_y})$ and replacing it in Eq. (23) we have

$$u_z(x,y) = \frac{1}{2}\left[1 + e^{-i2\pi(\frac{z}{z_{\mathrm{RT}}})} g(x,y)\right]. \tag{28}$$

Now, intensity and phase distributions in an arbitrary z can be calculated, respectively, by

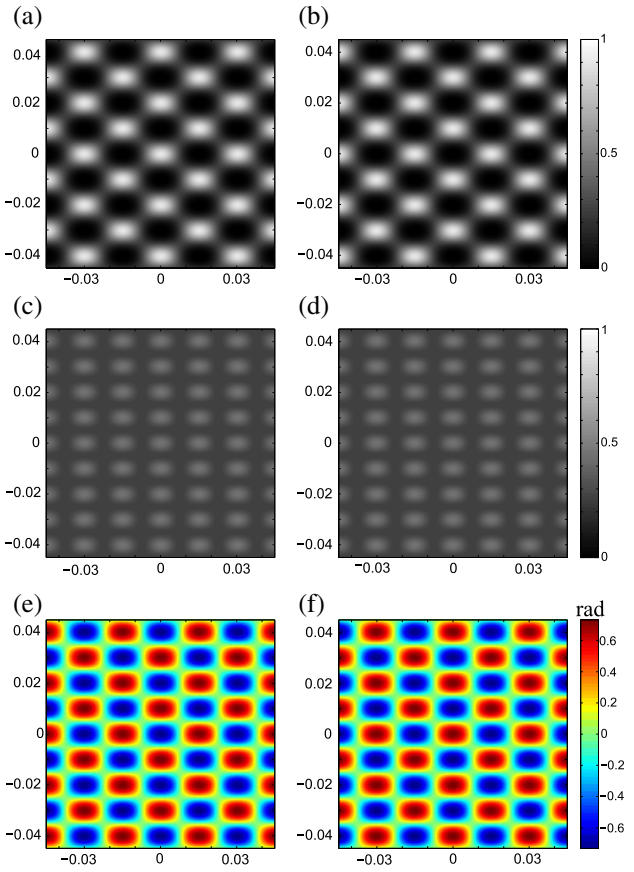

Fig. 3. Typical near-field intensity patterns of a 2D nonseparable sinusoidal grating with $p_x = 0.3$ mm and $p_y = 0.5$ mm at the (a) RT, (b) RHT, (c) RQT with an even n, and (d) RQT with an odd n, distances. (e) and (f) are the corresponding phase maps of (c) and (d), respectively (see Visualization 1).

$$I_z(x,y) = \frac{1}{4}\left[1 + g(x,y)^2 + 2g(x,y)\cos\left(\frac{2\pi z}{z_{\mathrm{RT}}}\right)\right], \tag{29}$$

$$\varphi_z(x,y) = \tan^{-1}\left[\frac{g(x,y)\sin\left(\frac{2\pi z}{z_{\mathrm{RT}}}\right)}{1 + g(x,y)\cos\left(\frac{2\pi z}{z_{\mathrm{RT}}}\right)}\right]. \tag{30}$$

Using Eq. (29) and the Michelson contrast definition,

$$C_I = \frac{I_{\max} - I_{\min}}{I_{\max} + I_{\min}}. \tag{31}$$

We can calculate contrast variation of the intensity pattern as a function of z. Similarly, we can define phase contrast by

$$C_\varphi = \frac{\varphi_{\max} - \varphi_{\min}}{\frac{\pi}{2}}. \tag{32}$$

In Fig. 4, the contrast variation of the intensity pattern and phase contrast are plotted in a z_{RT} distance. In the background visualization of Fig. 3, evolution of the diffraction patterns and contrast curves of typical 2D sinusoidal separable and nonseparable gratings are illustrated in a range of a $z_{\mathrm{lcm}}/2$ distance (Visualization 1). The phase contrast curve gets the form of a

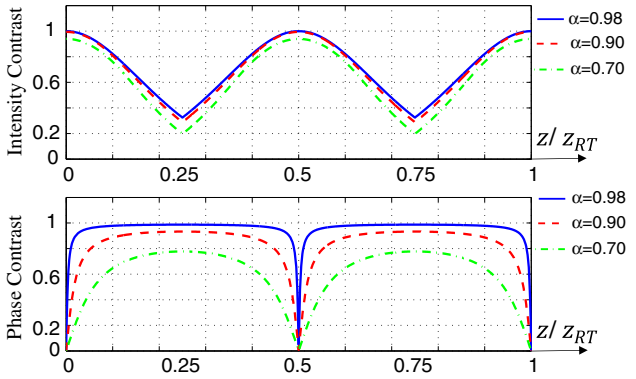

Fig. 4. Variation of intensity and phase contrasts for the near-field diffraction patterns of a 2D nonseparable sinusoidal grating in terms of z for three different values of α (see Visualization 2).

1D reversed Dirac comb when α tends toward 1 (see Fig. 4 and Visualization 2).

As another way to explain this odd result, the formation of self-images at a distance smaller than both z_{tx} and z_{tx}, we add Appendix A to the work. We know that all impulses of a 2D nonseparable sinusoidal grating except the DC one (at the spectral domain) locate on a circle with a radius of f, where

$$f^2 = f_x^2 + f_y^2; \tag{33}$$

see the fifth column of Fig. 2. On the other hand, it can be shown that for a given 2D structure having impulses only on a circle with radius f, the Talbot distance is given by $z_t = \frac{2}{\lambda f^2}$; see Appendix A. Multiplying both sides of Eq. (33) by $\frac{\lambda}{2}$ we obtain

$$\frac{1}{z_t} = \frac{1}{z_{tx}} + \frac{1}{z_{ty}}, \tag{34}$$

which easily leads to the RT distance, presented in Eq. (22).

It is worth noting that as illustrated in the fourth column of Fig. 2, for the AS case, the non-DC impulses are not necessarily located over a circle. Therefore, it is not expected that the above-mentioned reduction for the Talbot distances occur for these structures.

B. 2D Orthogonal Nonseparable Structure Having Fourier Coefficients Only with Odd Indices

Here we investigate the near-field diffraction from 2D orthogonal nonseparable periodic structures having Fourier coefficients only with odd indices except the DC term. In this regard, we consider the following form for the transmittance:

$$u_0(x,y) = t_{0,0} + \sum_{\substack{m=-\infty \\ \text{odd}}}^{+\infty}\sum_{\substack{n=-\infty \\ \text{odd}}}^{+\infty} t_{m,n} e^{2\pi i(mf_x x + nf_y y)}, \tag{35}$$

where "odd"s under the summations indicate that m and n are odd numbers. As none of the summations includes index 0, then $t_{m,0} = t_{0,n} = 0$ in double summation. It means that in the far field, all the impulses on the coordinate axes, excluding the DC one, vanish; therefore the structure presented by

Eq. (35) is necessarily nonseparable. Using Eq. (14), amplitude field distribution at distance z from the structure is given by

$$u_z(x,y) = t_{0,0} + \sum_{\substack{m=-\infty \\ \text{odd}}}^{+\infty} \times \sum_{\substack{n=-\infty \\ \text{odd}}}^{+\infty} t_{m,n} e^{-2\pi i\left(\frac{z}{z_{\text{lcm}}}\right)(lm^2+kn^2)} e^{2\pi i(mf_x x+nf_y y)}. \quad (36)$$

Comparing Eqs. (35) and (36), here again at distances equal to integer multiples of z_{lcm}, namely, $z_q = qz_{\text{lcm}}$, $q = 1, 2, 3, \ldots$, the light beam amplitude exactly recovers its initial form. Since the above expansions include only coefficients with odd indices, here some surprising results are obtained in some specific conditions.

Since l and k are relatively prime numbers, then both of them cannot be simultaneously even. There are two possibilities: one of l and k is odd and other one is even, or both of them are odd numbers. In the first case, $(lm^2 + kn^2)$ is an odd integer number, and therefore $z_t = z_{\text{lcm}}$. In the second case, where both l and k are odd integer numbers, $(lm^2 + kn^2)$ is an even integer number, and therefore $z_t = \frac{z_{\text{lcm}}}{2}$ can be regarded as the Talbot distance of the structure. This means that the Talbot distance halves. In the second case, some additional interesting facts can be revealed. From elementary number theory, it is known that the square of an odd integer number can be written in the form of $8q + 1$, where $q = 0, 1, 2, 3, \ldots$. Then we can write $m^2 = 8m' + 1$ and $n^2 = 8n' + 1$, and therefore,

$$(lm^2 + kn^2) = 8(lm' + kn') + (l + k). \quad (37)$$

Now let us follow the case if $(l + k)$ has a common factor with number 8. We will show that such a condition can be fulfilled by a suitable choice of p_x and p_y. The set of odd integer numbers can be classified into the following four groups:

$$(G1)8q + 1, \quad (G2)8q + 3, \quad (G3)8q + 5, \quad (G4)8q + 7, \quad (38)$$

where in all of groups $q = 0, 1, 2, 3, \ldots$. Now we consider all possible combinations of $l + k$ from the introduced groups. By the aid of the following 10 different combinations of the introduced groups, the number of theoretic properties of $l + k$ can be determined. For the values of $l + k$, there are 10 different cases, and we show these 10 cases by

$$(G1, G1), (G1, G2), (G1, G3), (G1, G4), (G2, G2), (G2, G3), (G2, G4), (G3, G3), (G3, G4), (G4, G4), \quad (39)$$

where, for instance, $(G2, G3)$ means that one of l or k belongs to the group $G2$ and the other one belongs to $G3$. In fact, all these 10 combinations can be categorized into the following three categories:

$$\begin{aligned} &\text{First category}: \{(G1, G1), (G1, G3), (G2, G2), \\ &\qquad (G2, G4), (G3, G3), (G4, G4)\}, \\ &\text{Second category}: \{(G1, G2), (G3, G4)\}, \\ &\text{Third category}: \{(G1, G4), (G2, G3)\}. \end{aligned} \quad (40)$$

The common factors of $(l + k)$ with number 8 for the first, second, and third categories, are equal to 2, 4, and 8, respectively. Therefore, the Talbot distance for the first, second, and third categories are $z_t = \frac{z_{\text{lcm}}}{2}$, $z_t = \frac{z_{\text{lcm}}}{4}$, and $z_t = \frac{z_{\text{lcm}}}{8}$, respectively. These results show that self-images of the checker gratings strongly depend on the values of l and k, and therefore on the ratio of their periods in the x and y directions.

In the following, we introduce two typical 2D orthogonal nonseparable periodic structures having Fourier coefficients with only odd indices. To construct such structures, we utilize two well-known square and triangle wave functions varying between −1 and 1; see [38].

Their Fourier expansion of square and triangle wave functions with period of p are given by

$$\text{Sq}(x;p) = \sum_{\substack{m=1 \\ \text{odd}}}^{+\infty} \frac{4}{m\pi} \sin\left(\frac{2m\pi x}{p}\right) \quad (41)$$

and

$$\text{Tr}(x,p) = \sum_{\substack{m=1 \\ \text{odd}}}^{+\infty} \frac{8}{(m\pi)^2} \cos\left(\frac{2m\pi x}{p}\right), \quad (42)$$

respectively. Using these functions, the two following 2D orthogonal nonseparable structures can be constructed:

$$t(x,y) = \frac{1}{2}[1 + \text{Sq}(x;p_x)\text{Sq}(y;p_y)], \quad (43)$$

$$t(x,y) = \frac{1}{2}[1 + \text{Tr}(x;p_x)\text{Tr}(y;p_y)], \quad (44)$$

where p_x and p_y are the structures' periods in the x and y directions, respectively. Considering Eqs. (41) and (42), these transmission functions are in the form of Eq. (35). In fact, Eq. (43) presents a checker grating. To realize the presented results, in the following we investigate self-imaging of the checker gratings with a different ratio of periods in the orthogonal directions. For each specified category, we present an example to show the predicted RT distances and additional results.

C. Diffraction from a Checker Grating As a 2D Orthogonal Nonseparable Periodic Structure

Here we investigate near-field diffraction from a checker grating as a typical example of 2D orthogonal nonseparable periodic structures having Fourier coefficients only with odd indices. In Fig. 5, a checker grating with nonequal periods in the x and y directions is illustrated. We describe a checker grating by the following transmission function:

$$t(x,y) = \frac{1}{2}\left\{1 + \text{sign}\left[\sin\left(\frac{2\pi x}{p_x}\right)\sin\left(\frac{2\pi y}{p_y}\right)\right]\right\}, \quad (45)$$

where "sign" indicates the sign function, which extracts the sign of a real number. This expression for a checker grating makes it easy to use in computational software such as MATLAB. Comparing Eqs. (45) and (9), one can consider this transmission function as the binary equivalent of 2D nonseparable sinusoidal structure defined by Eq. (9). This transmission

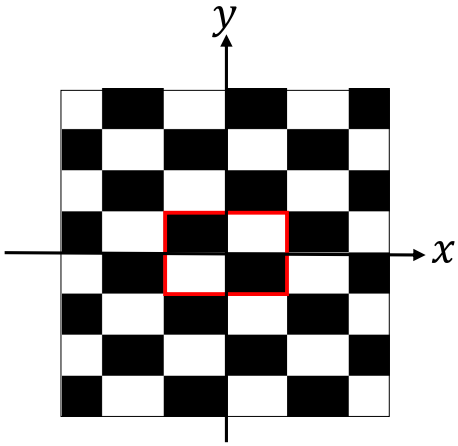

Fig. 5. Typical checker grating having nonequal periods in the x and y directions. A unit cell of the grating is shown by the red rectangle.

function and therefore the field distribution immediately after the grating can be written by the following Fourier expansion:

$$u_0(x,y)=\frac{1}{2}+\sum_{\substack{m=1\\ \text{odd}}}^{+\infty}\sum_{\substack{n=1\\ \text{odd}}}^{+\infty}\frac{8}{mn\pi^2}\sin\left(\frac{2\pi x}{p_x}\right)\sin\left(\frac{2\pi y}{p_y}\right). \quad \textbf{(46)}$$

Using Eq. (36), the amplitude field distribution at distance z from the grating is given by

$$u_z(x,y)=\frac{1}{2}+\sum_{\substack{m=1\\ \text{odd}}}^{+\infty}\sum_{\substack{n=1\\ \text{odd}}}^{+\infty}\frac{8}{mn\pi^2}e^{-2\pi i\left(\frac{z}{z_{\text{lcm}}}\right)(lm^2+kn^2)}\sin\left(\frac{2\pi x}{p_x}\right)\sin\left(\frac{2\pi y}{p_y}\right), \quad \textbf{(47)}$$

In Fig. 6, the near-field diffraction patterns of a checker grating with an even value l and odd value of k at different distances from the grating are illustrated. As can be seen, the self-images of the checker grating at the Talbot and half-Talbot distances are complementary to each other; see Figs. 6(a) and 6(b). Similar to the 1D Ronchi grating case [38], at the quarter-Talbot distances, $\frac{z_t}{4}$ and $\frac{3z_t}{4}$, uniform intensity patterns form; see Figs. 6(c) and 6(d). The corresponding phase patterns have checker profiles in which they are the negative of each other [Figs. 6(e) and 6(f)].

Figure 7 shows the near-field diffraction patterns of a checker grating with odd values l and k belonging into the first category introduced in Eq. (40)—say, $z_t=\frac{z_{\text{lcm}}}{2}$—at different distances from the grating. The same as in the case of

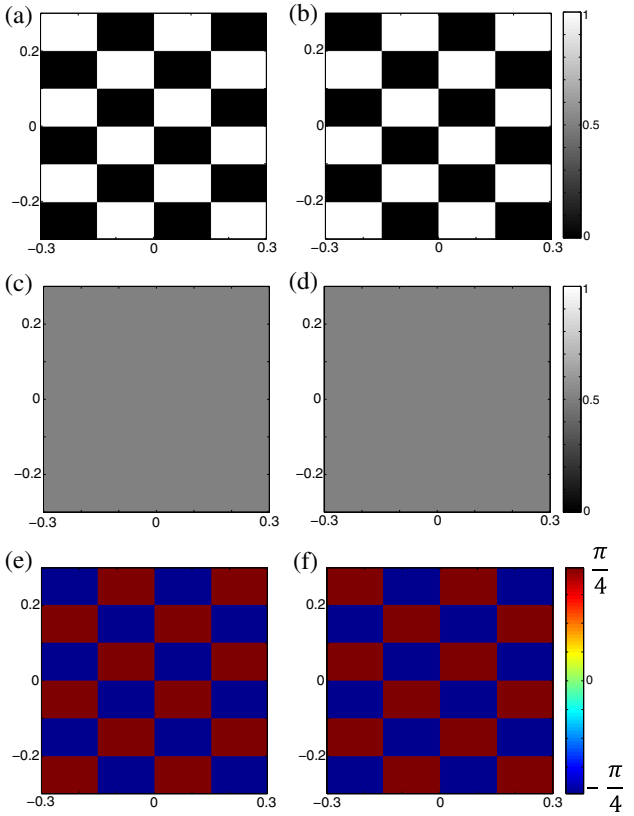

Fig. 6. Near-field diffraction patterns of a checker grating with $p_x=0.3$ mm, $p_y=0.2$ mm, and the respective values of $l=4$ and $k=9$. Intensity pattern immediately after the grating and (a) at the Talbot distance $z=z_t=z_{\text{lcm}}$, (b) at the half-Talbot distance $z=\frac{z_t}{2}$, (c) at the quarter-Talbot distance $z=\frac{z_t}{4}$, and (d) at the quarter-Talbot distance $z=\frac{3z_t}{4}$; respective phase patterns at the quarter-Talbot distances (e) $z=\frac{z_t}{4}$ and (f) $z=\frac{3z_t}{4}$.

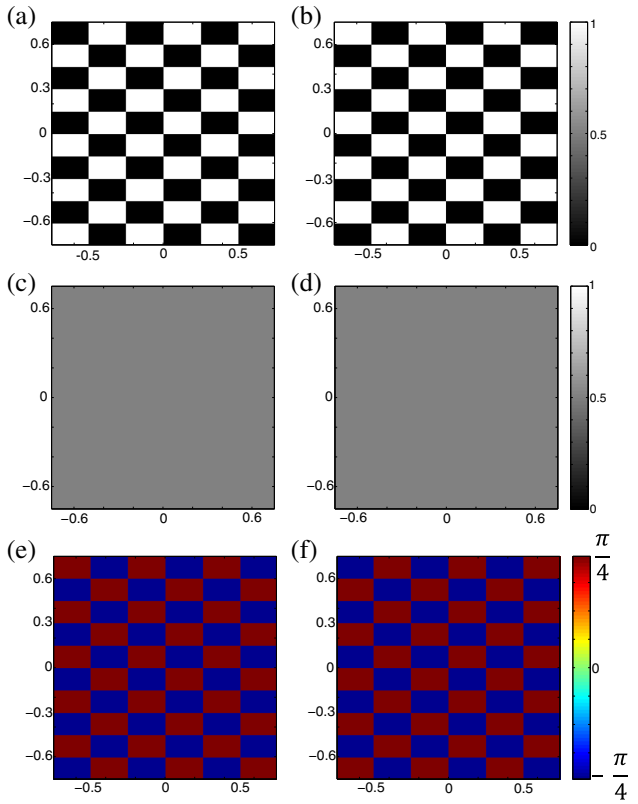

Fig. 7. Near-field diffraction patterns of a checker grating having $p_x=0.5$ mm, $p_y=0.3$ mm, and the respective values of $l=9$ and $k=25$; intensity pattern immediately after the grating and (a) at the Talbot distance $z=z_t=\frac{z_{\text{lcm}}}{2}$, (b) at the half-Talbot distance $z=\frac{z_t}{2}$, (c) at the quarter-Talbot distance $z=\frac{z_t}{4}$, and (d) at the quarter-Talbot distance $z=\frac{3z_t}{4}$; corresponding phase patterns at the quarter-Talbot distances (e) $z=\frac{z_t}{4}$ and (f) $z=\frac{3z_t}{4}$.

Fig. 6, here the respective self-images at the Talbot and half-Talbot distances are complementary to each other; at the quarter-Talbot distances uniform intensity patterns form, and the phase patterns have checker profiles in which they are the negative of each other.

Figure 8 presents the near-field diffraction patterns of a checker grating with odd values l and k belonging into the second category introduced in Eq. (40)—say, $z_t = \frac{z_{\mathrm{lcm}}}{4}$—at different distances from the grating. As is apparent, the self-images of the structure at the respective Talbot and half-Talbot distances are complementary to each other; see Figs. 8(a) and 8(b). At both quarter-Talbot distances, $\frac{z_t}{4}$ and $\frac{3z_t}{4}$, after subtracting the background intensity, a 2D MS periodic intensity pattern is formed; see Figs. 6(c) and 6(d). Here, the period of the intensity patterns is halved. The corresponding phase patterns have three-level profiles in which they are the negative of each other [Figs. 8(e) and 8(f)]. Unlike the respective intensity profiles, here the period of the phase patterns is equal to the period of the structure.

Figure 9 presents the same patterns as Fig. 8 for a checker grating belonging to the third category introduced in Eq. (40)—say, $z_t = \frac{z_{\mathrm{lcm}}}{8}$—at different distances from the grating. As is shown in Figs. 9(a) and 9(b), here the diffraction patterns at the respective Talbot and half-Talbot distances are not similar. Here, at the half-Talbot distances, the intensity patterns are checker-like patterns in which the filling factor is decreased. Therefore the value of intensity over the bright areas is larger than its value over the self-image planes. This feature can be found in applications in lithography, optical manipulation, etc. At the quarter-Talbot distances, both the intensity and phase profiles are the same period of the structure, but they have elaborate structures; see Figs. 9(c)–9(f). The intensity patterns at the $\frac{z_t}{4}$ and $\frac{3z_t}{4}$ are the same, but their phase profiles are the negative of each other's.

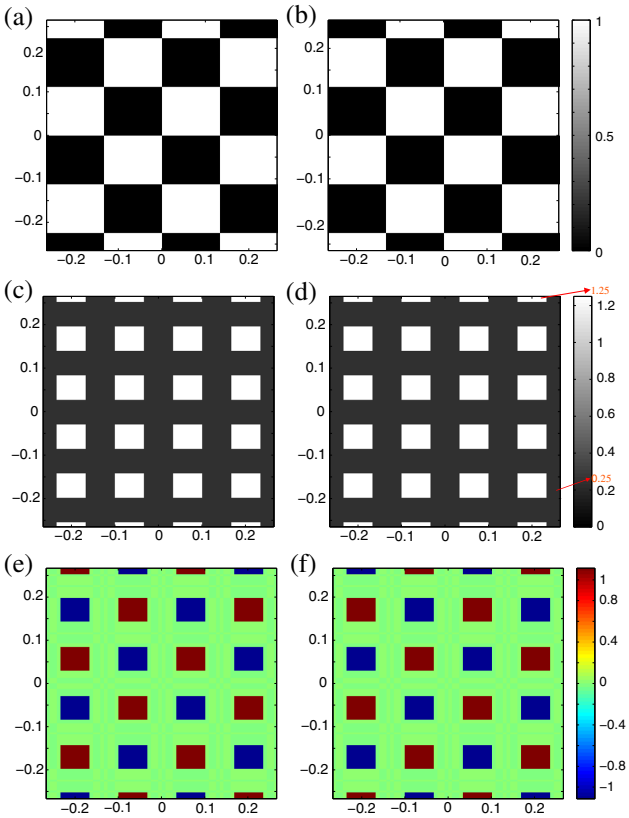

Fig. 8. Near-field diffraction patterns of a checker grating with $p_x = \sqrt{7} \times 10^{-1}$ mm, $p_y = \sqrt{5} \times 10^{-1}$ mm, and corresponding values of $l = 5$ and $k = 7$; intensity pattern immediately after the grating and at the Talbot distance (a) $z = z_t = \frac{z_{\mathrm{lcm}}}{4}$, (b) at the half-Talbot distance $z = \frac{z_t}{2}$, (c) at the quarter-Talbot distance $z = \frac{z_t}{4}$, and at the quarter-Talbot distance (d) $z = \frac{3z_t}{4}$; respective phase patterns at the quarter-Talbot distances (e) $z = \frac{z_t}{4}$ and (f) $z = \frac{3z_t}{4}$.

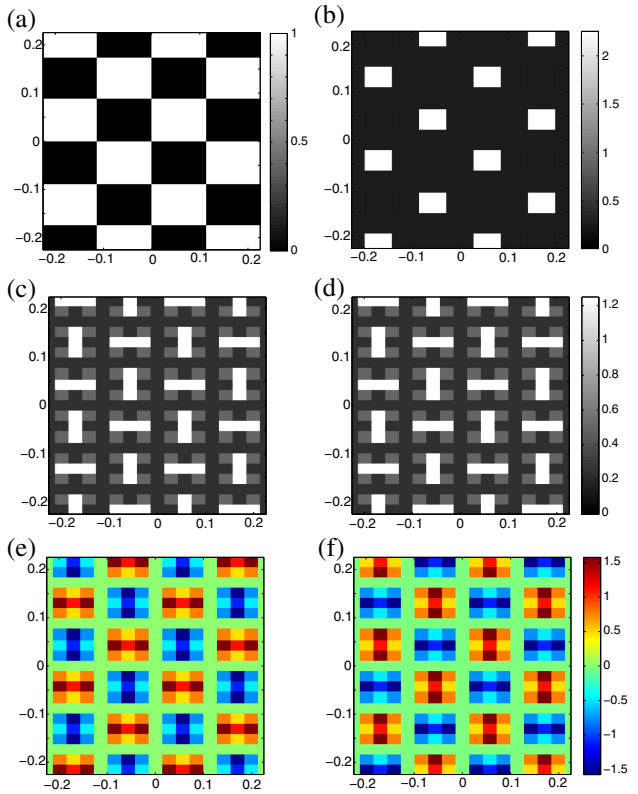

Fig. 9. Near-field diffraction patterns of a checker grating with $p_x = \sqrt{5} \times 10^{-1}$ mm, $p_y = \sqrt{3} \times 10^{-1}$ mm, $l = 3$, and $k = 5$; intensity pattern immediately after the grating and (a) at the Talbot distance $z = z_t = \frac{z_{\mathrm{lcm}}}{8}$, (b) at the half-Talbot distance $z = \frac{z_t}{2}$, (c) at the quarter-Talbot distance $z = \frac{z_t}{4}$, and (d) at the quarter-Talbot distance $z = \frac{3z_t}{4}$; respective phase patterns at the quarter-Talbot distances (e) $z = \frac{z_t}{4}$ and (f) $z = \frac{3z_t}{4}$.

5. CONCLUSION

In this work, based on the spatial spectrum of a 2D periodic structure, its orthogonality and separability into two 1D structures were determined. For the first time, for a 2D orthogonal nonseparable grating with sinusoidal profile, the self-images, negative self-images, and subimages formation conditions and their characterizations were presented. Also, for the 2D orthogonal nonseparable periodic structures having Fourier coefficients only with odd indices, it was shown that the Talbot distance strongly depends on the number theoretic properties of the structure.

In Appendix A of the work, formation of self-images for 2D almost periodic structures having impulses on zone-plate-like concentric circles at the spectral domain is predicted, and the Talbot distance is determined in terms of the first circle's radius.

The near-field diffraction from 2D structures separable in the polar coordinates has recently found interesting applications [39–42]. It seems that the diffraction from 2D structures that are periodic along both radial and azimuthal directions also leads to new achievements.

APPENDIX A

A. Talbot Effect of 2D Almost Periodic Structures

Here we consider the near-field diffraction from 2D almost periodic structures and discover a sufficient condition for the almost periodic structures in which they have self-images under coherent plane wave illumination. A 2D structure is almost periodic when it has a 2D almost periodic transmission function. The Fourier series representation of an almost periodic transmission function $t(x,y)$ is [9]

$$t(x,y) = \sum_{n=0}^{\infty} t_n \exp(i2\pi \vec{f}_n.\vec{r}) = t_0 + \sum_{n=1}^{\infty} t_n \exp[i2\pi(f_{nx}x + f_{ny}y)], \quad \textbf{(A1)}$$

where $\vec{f}_n = (f_{nx}, f_{ny})$ indicates an arbitrary point in the spectrum domain and $\vec{r} = (x,y)$, and $n = 0$ corresponds to the DC term with $\vec{f}_0 = (f_{0x}, f_{0y}) = (0,0)$ located at the spectrum origin. By illuminating the structure with a coherent uniform light beam, the field distribution immediately after the structure is $u_0(x,y) = t(x,y)$, and the corresponding spatial spectrum is

$$U_0(\xi,\eta) = \sum_{n=0}^{\infty} t_n \delta(\xi - f_{nx}, \eta - f_{ny}). \quad \textbf{(A2)}$$

Multiplying this expression to the free space transfer function, $H(\xi,\eta) = H_0 \exp[-i\pi\lambda z(\xi^2+\eta^2)]$, at a distance z from the structure, the spatial spectrum is given by

$$U_z(\xi,\eta) = \sum_{n=0}^{\infty} t_n \exp[-i\pi\lambda z(\xi^2+\eta^2)] \times \delta(\xi - f_{nx}, \eta - f_{ny}). \quad \textbf{(A3)}$$

The amplitude field distribution at z obtains by taking the 2D inverse Fourier transform of Eq. (A3):

$$u_z(x,y) = t_0 + \sum_{n=1}^{+\infty} t_n \exp[i2\pi(f_{nx}x + f_{ny}y)] \times \exp[-i\pi\lambda z(f_{nx}^2 + f_{ny}^2)]. \quad \textbf{(A4)}$$

When the set of impulses in the spatial spectrum domain forms a 2D orthogonal lattice—say, $\vec{f}_{m,n} = (mf_x, nf_y)$—the structures is a 2D orthogonal periodic structure, which is discussed in the third section of the paper. Here we propose another arrangement of impulses. Suppose that all of impulses are located on a circle around the spectrum origin with radius f, except the DC one. Therefore, we have $f_{nx}^2 + f_{ny}^2 = f^2$, and Eq. (A4) can be rewritten as follows:

$$u_z(x,y) = t_0 + e^{-i2\pi\frac{z}{z_t}} \sum_{n=1}^{+\infty} t_n e^{i2\pi(f_{nx}x + f_{ny}y)}, \quad \textbf{(A5)}$$

where $z_t = \frac{2}{\lambda f^2}$ is the structure's Talbot distance. Comparing Eq. (A5) with Eq. (A1), one can deduce that at distances equal to integer multiples of z_t, say, $z_q = qz_t$, $q = 1, 2, 3, \ldots$, the light beam amplitude exactly recovers its initial shape.

B. Diffraction from Pure Amplitude Octagonal Sinusoidal Structure

To clarify the matter, we construct a structure so that its spectrum impulses are located at the center and vertices of an octagon on the spectral domain; see Fig. 10(b). Considering $t_0 = \frac{1}{2}$ and the other eight coefficients $t_n = \frac{1}{8}$ in Eq. (A1), we obtain

$$t(x,y) = \frac{1}{2}[1 + g(x,y)], \quad \textbf{(A6)}$$

in which

$$g(x,y) = \frac{\alpha}{4}\cos(2\pi f x) + \frac{\alpha}{4}\cos(2\pi f y) + \frac{\alpha}{4}\cos(\sqrt{2}\pi f(x+y)) + \frac{\alpha}{4}\cos(\sqrt{2}\pi f(x-y)). \quad \textbf{(A7)}$$

In Fig. 10(a), this transmission function is depicted. Using Eq. (A5), the complex amplitude of diffracted light is

$$u_z(x,y) = \frac{1}{2}\left[1 + e^{-i2\pi\frac{z}{z_t}} g(x,y)\right]. \quad \textbf{(A8)}$$

Using this result, the diffracted intensity patterns at $z = z_t$ and $z = \frac{z_t}{2}$ are illustrated in Figs. 10(c) and 10(d), respectively. The intensity patterns at the Talbot and half-Talbot distances are almost the negative of each other. In the background movie

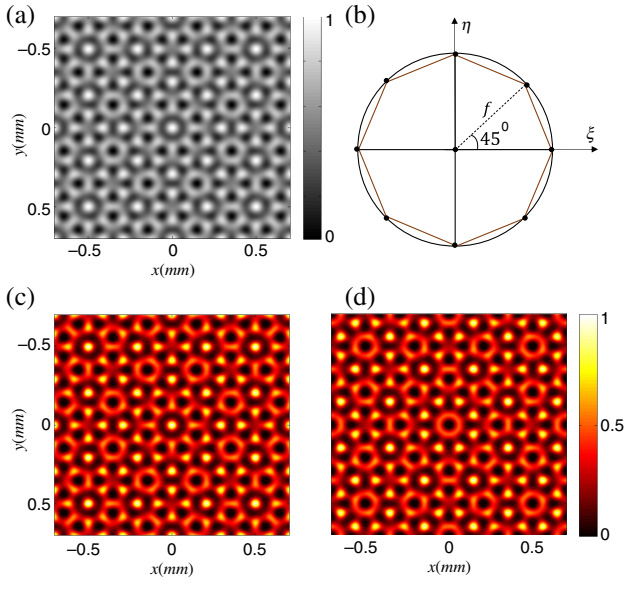

Fig. 10. Pure amplitude octagonal sinusoidal structure. (a) Transmission function, (b) its impulse-comb in the spectral domain; (c) the intensity patterns immediately after the structure and at the Talbot distances; and (d) the intensity patterns at the half-Talbot distances; see Visualization 3.

of Fig. 10, Visualization 3, the diffraction patterns from a pure amplitude octagonal sinusoidal structure, under propagation in a range of a z_t (left) and the corresponding phase maps (right) are presented. Using the definitions of Eqs. (31) and (32), their corresponding contrast curves are calculated and shown in the following rows. The fundamental spatial frequency of the structure is $f = 10\ \text{mm}^{-1}$ and $\alpha = 0.95$.

C. 2D Almost Periodic Structures Having Impulses Located on Zone-Plate-Like Concentric Circles

We consider a generalized case in which the spectral impulses of the structure are located on zone-plate-like concentric circles. In this case, all impulses, excluding the DC one, locate on a family of concentric circles around the spectrum origin so that the radius of the mth circle, f_m, is proportional to $\sqrt{m}$, say, $f_m = \sqrt{m}f$, where f is the radius of the central circle or equally is the fundamental spatial frequency of the structure. We show the location of the nth impulse on the mth spectral circle by $\vec{f}_{mn} = (f_{mnx}, f_{mny})$; then

$$f_{mnx}^2 + f_{mny}^2 = mf^2. \tag{A9}$$

This equation implies that this family of concentric circles constructs a zone plate in the spectrum domain. Strictly speaking, in this case Eq. (A1) gets the following form:

$$\begin{aligned} u_0(x,y) &= t_{00} + \sum_{m=1}^{\infty}\sum_{n=1}^{N_m} t_{mn}\ \exp(i2\pi\vec{f}_{mn}.\vec{r}) \\ &= t_{00} + \sum_{m=1}^{\infty}\sum_{n=1}^{N_m} t_{mn}\ \exp[i2\pi(f_{mnx}x + f_{mny}y)], \end{aligned} \tag{A10}$$

where N_m is the number of impulses on the mth spectrum circle. In a similar way, the complex amplitude of the diffracted light at distance z from the structure is obtained as follows:

$$\begin{aligned} u_z(x,y) = t_{00} &+ \sum_{m=1}^{\infty}\sum_{n=1}^{N_m} t_{mn}\ \exp[i2\pi(f_{mnx}x + f_{mny}y)] \\ &\times \exp[-i\pi\lambda z(f_{mnx}^2 + f_{mny}^2)]. \end{aligned} \tag{A11}$$

Substituting Eq. (A9) in Eq. (A11), we get

$$u_z(x,y) = t_{00} + \sum_{m=1}^{\infty}\sum_{n=1}^{N_m} t_{mn} e^{i2\pi(f_{mnx}x + f_{mny}y)} e^{-i2m\pi\frac{z}{z_t}}, \tag{A12}$$

where $z_t = \frac{2}{\lambda f^2}$ is the Talbot distance. Comparing Eq. (A12) with Eq. (A10), we see that at distances equal to integer multiples of z_t, say, $z_q = qz_t$, $q = 1, 2, 3, \ldots$, the light beam amplitude exactly recovers its initial shape.

As an interesting example, we come back again to a 2D orthogonal periodic structure. Impulses of this structure in the spectrum domain form a 2D orthogonal lattice in which (m, n)th impulse can be specified by

$$\vec{f}_{mn} = mf_x\hat{\boldsymbol{x}} + nf_y\hat{\boldsymbol{y}}, \tag{A13a}$$

$$f_{m,n}^2 = (mf_x)^2 + (nf_y)^2, \tag{A13b}$$

where $\hat{\boldsymbol{x}}$ and $\hat{\boldsymbol{y}}$ are the Cartesian unit vectors, and $f_x = \frac{1}{p_x}$ and $f_y = \frac{1}{p_y}$ are the fundamental frequencies of the structure in the x and y directions, respectively. Here we determine a sufficient condition for p_x and p_y of the structure so that all impulses of the structure locate on zone-plate-like concentric circles. If $p_x = \sqrt{q}p_y$, where $q = 1, 2, 3, \ldots$, then $f_y = \sqrt{q}f_x$. Now, substituting $f_y = \sqrt{q}f_x$ in Eq. (A13b), we get

$$f_{m,n} = \sqrt{m^2 + qn^2}f_x = \sqrt{k}f_x, \tag{A14}$$

where $k = m^2 + qn^2$ is obviously a positive integer. In this case, all impulses of the structure are located on zone-plate-like concentric circles, and therefore for this structure the Talbot distance is independent of p_y, say, $z_t = z_{tx} = \frac{2p_x^2}{\lambda}$.

Funding. Institute for Advanced Studies in Basic Sciences (IASBS) Research Council (G2016IASBS12632, G2018IASBS12632).

REFERENCES

1. S. Yokozeki and T. Suzuki, "Shearing interferometer using the grating as the beam splitter," Appl. Opt. **10**, 1575–1580 (1971).
2. S. Rasouli and M. Ghorbani, "Nonlinear refractive index measuring using a double-grating interferometer in pump-probe configuration and Fourier transform analysis," J. Opt. **14**, 035203 (2012).
3. S. Rasouli, F. Sakha, and M. Yeganeh, "Infinite-mode double-grating interferometer for investigating thermal-lens–acting fluid dynamics," Meas. Sci. Technol. **29**, 085201 (2018).
4. M. M. Alkaisi, R. J. Blaikie, S. J. McNab, R. Cheung, and D. R. S. Cumming, "Sub-diffraction-limited patterning using evanescent near-field optical lithography," Appl. Phys. Lett. **75**, 3560–3562 (1999).
5. D. Thomae, O. Sandfuchs, and R. Brunner, "Quantitative analysis of imperfect frequency multiplying in fractional Talbot planes and its effect on high-frequency-grating lithography," J. Opt. Soc. Am. A **31**, 1436–1444 (2014).
6. A. Naqavi, H. Peter Herzig, and M. Rossi, "High-contrast self-imaging with ordered optical elements," J. Opt. Soc. Am. B **33**, 2374–2382 (2016).
7. K. Patorski and M. Kujawinska, *Handbook of the Moiré Fringe Technique* (Elsevier, 1993).
8. C. A. Walker, *Handbook of Moiré Measurement* (CRC Press, 2003).
9. I. Amidror, *Theory of the Moiré Phenomenon* (Springer, 2007), Vols. **I–II**.
10. M. Yeganeh and S. Rasouli, "Moiré fringes of higher-order harmonics versus higher-order moiré patterns," Appl. Opt. **57**, 9777–9788 (2018).
11. S. Rasouli and M. Shahmohammadi, "A portable and long-range displacement and vibration sensor that chases moving moiré fringes using the three-point intensity detection method," OSA Continuum **1**, 1012–1025 (2018).
12. V. Saveljev, S.-K. Kim, H. Lee, H.-W. Kim, and B. Lee, "Maximum and minimum amplitudes of the moiré patterns in one- and two-dimensional binary gratings in relation to the opening ratio," Opt. Express **24**, 2905–2918 (2016).
13. V. Saveljev, S. K. Kim, and J. Kim, "Moiré effect in displays: a tutorial," Opt. Eng. **57**, 030803 (2018).
14. H. F. Talbot, "Facts relating to optical science, No. IV," Philos. Mag. **9**(56), 401–407 (1836).
15. J. Cowley and A. Moodie, "Fourier images IV: the phase grating," Proc. Phys. Soc. London **76**, 378–384 (1960).
16. W. D. Montgomery, "Self-imaging objects of infinite aperture," J. Opt. Soc. Am. **57**, 772–778 (1967).
17. L. Rayleigh, "On copying diffraction-gratings, and on some phenomena connected herewith," Philos. Mag. **11**(67), 196–205 (1881).
18. K. Patorski, L. Wronkowski, and M. Dobosz, "Some properties of Fresnel images of a square wave amplitude grating," J. Mod. Opt. **29**, 565–567 (1982).

19. K. Patorski, "Self-imaging phenomenon lateral shift of Fresnel images," J. Mod. Opt. **30**, 1255–1258 (1983).
20. P. Szwaykowski, "The lateral shift of Fresnel images of periodic objects under coherent plane wave illumination," J. Mod. Opt. **31**, 563–566 (1984).
21. K. Patorski, "I the self-imaging phenomenon and its applications," Prog. Opt. **27**, 1–108 (1989).
22. H. Hamam and J. L. de Bougrenet de la Tocnaye, "Fractional Talbot four-level phase-only holograms using ferroelectric liquid-crystal spatial light modulators," Opt. Lett. **19**, 1654–1656 (1994).
23. H. Hamam and J. L. de Bougrenet de la Tocnaye, "Efficient Fresnel transform algorithm based on fractional Fresnel diffraction," J. Opt. Soc. Am. A **12**, 1920–1931 (1995).
24. M. V. Berry and S. Klein, "Integer, fractional and fractal Talbot effects," J. Mod. Opt. **43**, 2139–2164 (1996).
25. S. Bhattacharya and R. S. Sirohi, "Amplitude checker grating from one-dimensional Ronchi grating and its application to array generation," Appl. Opt. **36**, 3745–3752 (1997).
26. H. Hamam, "Talbot array illuminators: general approach," Appl. Opt. **36**, 2319–2327 (1997).
27. V. Arrizon and G. Rojo-Velazquez, "Fractional Talbot field of finite gratings: compact analytical formulation," J. Opt. Soc. Am. A **18**, 1252–1256 (2001).
28. H. Hamam, "Talbot imaging and unification," Appl. Opt. **42**, 7052–7059 (2003).
29. A. W. Lohmann, H. Knuppertz, and J. Jahns, "Fractional Montgomery effect: a self-imaging phenomenon," J. Opt. Soc. Am. A **22**, 1500–1508 (2005).
30. J. Wen, Y. Zhang, and M. Xiao, "The Talbot effect: recent advances in classical optics, nonlinear optics, and quantum optics," Adv. Opt. Photon. **5**, 83–130 (2013).
31. K. Pelka, J. Graf, T. Mehringer, and J. von Zanthier, "Prime number decomposition using the Talbot effect," Opt. Express **26**, 15009–15014 (2018).
32. J. L. Flores, B. Bravo-Medina, and J. A. Ferrari, "One-frame two-dimensional deflectometry for phase retrieval by addition of orthogonal fringe patterns," Appl. Opt. **52**, 6537–6542 (2013).
33. K. Patorski, M. Trusiak, and K. Pokorski, "Single-shot two-channel Talbot interferometry using checker grating and Hilbert-Huang fringe pattern processing," Proc. SPIE **9132**, 91320Z (2014).
34. P. Han and J. Weng, "Talbot images and Talbot spectra of a 2D orthogonal periodicity structure," J. Opt. **18**, 055606 (2016).
35. S. Rasouli, D. Hebri, and A. M. Khazaei, "Investigation of various behaviors of near- and far-field diffractions from multiplicatively separable structures in the x and y directions, and a detailed study of the near-field diffraction patterns of 2D multiplicatively separable periodic structures using the contrast variation method," J. Opt. **19**, 095601 (2017).
36. K. Patorski, L. Sluzewski, and M. Trusiak, "5-beam grating interferometry for extended phase gradient sensing," Opt. Express **26**, 26872–26887 (2018).
37. J. W. Goodman, *Introduction to Fourier Optics*, 2nd ed. (McGraw-Hill, 1996).
38. S. Rasouli and D. Hebri, "Contrast enhanced quarter-Talbot images," J. Opt. Soc. Am. A **34**, 2145–2156 (2017).
39. S. Rasouli, A. M. Khazaei, and D. Hebri, "Talbot carpet at the transverse plane produced in the diffraction of plane wave from amplitude radial gratings," J. Opt. Soc. Am. A **35**, 55–64 (2018).
40. D. Hebri, S. Rasouli, and M. Yeganeh, "Intensity-based measuring of the topological charge alteration by the diffraction of vortex beams from amplitude sinusoidal radial gratings," J. Opt. Soc. Am. B **35**, 724–730 (2018).
41. S. Rasouli, A. M. Khazaei, and D. Hebri, "Radial carpet beams: a class of nondiffracting, accelerating, and self-healing beams," Phys. Rev. A **97**, 033844 (2018).
42. D. Hebri and S. Rasouli, "Combined half-integer Bessel-like beams: a set of solutions of the wave equation," Phys. Rev. A **98**, 003800 (2018).